Monthly Notices
of the
ROYAL ASTRONOMICAL SOCIETY

MNRAS **463,** 2986–2996 (2016) doi:10.1093/mnras/stw2204
Advance Access publication 2016 September 2

Galaxy Zoo: evidence for rapid, recent quenching within a population of AGN host galaxies★

R. J. Smethurst,[1]† C. J. Lintott,[1] B. D. Simmons,[1,2]‡ K. Schawinski,[3] S. P. Bamford,[4] C. N. Cardamone,[5] S. J. Kruk,[1] K. L. Masters,[6] C. M. Urry,[7] K. W. Willett[8] and O. I. Wong[9]

[1]*Department of Physics, Oxford Astrophysics, University of Oxford, Denys Wilkinson Building, Keble Road, Oxford OX1 3RH, UK*
[2]*Department of Physics, Center for Astrophysics and Space Sciences (CASS), University of California, San Diego, CA 92093, USA*
[3]*Department of Physics, Institute for Astronomy, ETH Zürich, Wolfgang-Pauli Strasse 27, CH-8093 Zürich, Switzerland*
[4]*School of Physics and Astronomy, The University of Nottingham, University Park, Nottingham NG7 2RD, UK*
[5]*Math and Science Department, Wheelock College, 200 The Riverway, Boston, MA 02215, USA*
[6]*Institute of Cosmology and Gravitation, University of Portsmouth, Dennis Sciama Building, Barnaby Road, Portsmouth PO1 3FX, UK*
[7]*Department of Physics and Yale Center for Astronomy and Astrophysics, Yale University, PO Box 208121, New Haven, CT 06520-8121, USA*
[8]*School of Physics and Astronomy, University of Minnesota, 116 Church St SE, Minneapolis, MN 55455, USA*
[9]*International Centre for Radio Astronomy Research, UWA, 35 Stirling Highway, Crawley, WA 6009, Australia*

Accepted 2016 August 31. Received 2016 August 31; in original form 2015 August 4

ABSTRACT

We present a population study of the star formation history of 1244 Type 2 active galactic nuclei (AGN) host galaxies, compared to 6107 inactive galaxies. A Bayesian method is used to determine individual galaxy star formation histories, which are then collated to visualize the distribution for quenching and quenched galaxies within each population. We find evidence for some of the Type 2 AGN host galaxies having undergone a rapid drop in their star formation rate within the last 2 Gyr. AGN feedback is therefore important at least for this population of galaxies. This result is not seen for the quenching and quenched inactive galaxies whose star formation histories are dominated by the effects of downsizing at earlier epochs, a secondary effect for the AGN host galaxies. We show that histories of rapid quenching cannot account fully for the quenching of all the star formation in a galaxy's lifetime across the population of quenched AGN host galaxies, and that histories of slower quenching, attributed to secular (non-violent) evolution, are also key in their evolution. This is in agreement with recent results showing that both merger-driven and non-merger processes are contributing to the co-evolution of galaxies and supermassive black holes. The availability of gas in the reservoirs of a galaxy, and its ability to be replenished, appear to be the key drivers behind this co-evolution.

Key words: galaxies: active – galaxies: evolution – galaxies: photometry – galaxies: Seyfert – galaxies: statistics.

1 INTRODUCTION

The nature of the observed co-evolution of galaxies and their central supermassive black holes (Magorrian et al. 1998; Marconi & Hunt 2003; Haring & Rix 2004) and the effects of active galactic nuclei (AGN) feedback on galaxies are two of the most important open issues in galaxy evolution. AGN feedback was first suggested as a mechanism for regulating star formation (SF) in simulations (Silk & Rees 1998; Bower et al. 2006; Croton et al. 2006; Somerville et al. 2008) and indirect evidence has been observed for both positive and negative feedback in various systems (see the comprehensive review from Fabian 2006).

The strongest observational evidence for AGN feedback in a population is that the largest fraction of AGN are found in the green valley (Cowie & Barger 2008; Hickox et al. 2009; Schawinski et al. 2010), suggesting some link between AGN activity and the process of quenching which moves a galaxy from the blue cloud to the red sequence. However, concrete statistical evidence for the effect of AGN feedback on the host galaxy population has so far been elusive.

Here we present a large observational population study of the star formation histories (SFHs) of Type 2 AGN host galaxies. We use a new Bayesian method (Smethurst et al. 2015) to effectively

★ This investigation has been made possible by the participation of over 350 000 users in the Galaxy Zoo project. Their contributions are acknowledged at http://authors.galaxyzoo.org.

† E-mail: rebecca.smethurst@astro.ox.ac.uk
‡ Einstein Fellow.

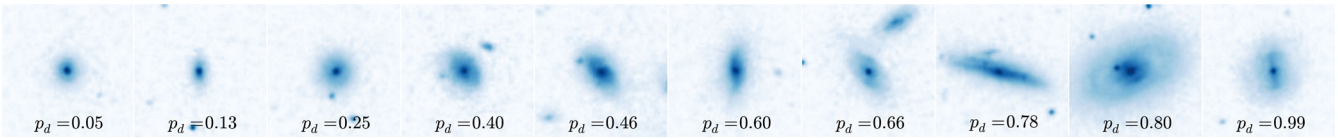

Figure 1. Randomly selected SDSS *gri* composite images from the sample of 1244 Type 2 AGN in a redshift range $0.04 < z < 0.05$. The galaxies are ordered from least to most featured according to their debiased 'disc or featured' vote fraction, $p_{\rm d}$ (see Willett et al. 2013). The scale for each image is 0.099 arcsec pixel^{-1}.

determine the most probable SFH of a galaxy, modelled with two parameters, time of quenching, $t_{\rm q}$, and exponential rate, τ, given the observed near-ultraviolet (NUV) and optical colours. This builds on the work of Martin et al. (2007) and Schawinski et al. (2014), but improves significantly on previous techniques. We aim to determine the following: (i) are galaxies currently hosting an AGN undergoing quenching? (ii) If so, when and at what rate does this quenching occur? (iii) Is this quenching occurring at different times and rates compared to a control sample of inactive galaxies?

The zero-points of all magnitudes are in the AB system. Where necessary, we adopt the *WMAP* Seven-Year Cosmology (Jarosik et al. 2011) with $(\Omega_{\rm m}, \Omega_\Lambda, h) = (0.26, 0.73, 0.71)$.

2 DATA AND METHODS

2.1 Data sources

In this investigation, we use visual classifications of galaxy morphologies from the Galaxy Zoo 2[1] (GZ2) citizen science project (Willett et al. 2013), which obtains multiple independent classifications for each optical image. The full question tree for an image is shown in fig. 1 of Willett et al. The GZ2 project used 304 022 images from the Sloan Digital Sky Survey Data Release 7 (SDSS; York et al. 2000; Abazajian et al. 2009) all classified by at least 17 independent users, with a mean number of classifications of ∼42.

Further to this, we required NUV photometry from the GALEX survey (Martin et al. 2005), within which ∼42 per cent of the GZ2 sample was observed, giving 126 316 galaxies in total ($0.01 < z < 0.25$). This will be referred to as the GZ2-GALEX sample. The completeness of this sample ($-22 < M_u < -15$) is shown in fig. 2 of Smethurst et al. (2015).

Observed fluxes are corrected for galactic extinction (Oh et al. 2011) by applying the Cardelli et al. (1989) law. We also adopt k-corrections to $z = 0.0$ and obtain absolute magnitudes from the NYU-VAGC (Blanton et al. 2005; Padmanabhan et al. 2008; Blanton & Roweis 2007).

2.2 AGN sample

We selected Type 2 AGN using a BPT diagram (Baldwin, Phillips & Terlevich 1981) using line and continuum strengths for [O III], [N II], [S II] and [O II] obtained from the MPA-JHU catalogue (Kauffman et al. 2003a; Brinchmann et al. 2004) for galaxies in the GZ2-GALEX sample. We then required the S/N > 3 for each emission line as in Schawinski et al. (2010). Those galaxies which satisfied all of the inequalities defined in Kewley et al. (2001) and Kauffman et al. (2003b) were selected as Type 2 AGN, giving 1299 host galaxies (∼10 per cent of the GZ2-GALEX sample). Sarzi et al. (2010), Yan & Blanton (2012) and Singh et al. (2013) have all demonstrated that low-ionization nuclear emission-line regions (LINERs) are not primarily powered by AGN, therefore for purity, we excluded these galaxies from the sample using the definition from Kewley et al. (2006) (55 galaxies total) with no change to the results. These 1244 galaxies will be referred to as the AGN-HOST sample.

We refrain from using Type 1 AGN due to concerns about contamination of the SFH analysis from potentially strong NUV emission by unobscured nuclei. The obscuration of Type 2 AGN is highly efficient, considerably more so in the NUV than the optical (Simmons et al. 2011); residual NUV flux from a Type 2 AGN can be neglected in comparison to that of the galaxy. We also investigated the possibility of contamination of optical galaxy colours by residual AGN emission, finding that subtracting measured nuclear magnitudes (SDSS `psfMag`) produces a negligible change in host galaxy colour ($\Delta(u-r) \sim 0.09$). We therefore use the uncorrected colours to avoid unnecessary complexity and minimize the propagation of uncertainty from the colours through to the SFHs. However, we note that including these corrected colours does not change our results.

We note also that galaxy colours were not corrected for intrinsic dust attenuation. This is of particular consequence for disc galaxies, where attenuation increases with increasing inclination. Buat et al. (2005) found the median value of the attenuation in the *GALEX* NUV passband to be ∼1 mag. Similarly, Masters et al. (2010) found a total extinction from face-on to edge-on spirals of 0.7 and 0.5 mag for the SDSS u and r passbands and show spirals with $\log(a/b) > 0.7$ have signs of significant dust attenuation. For the AGN-HOST (INACTIVE) sample, we find 23 per cent (25 per cent) of discs (with $p_d > 0.5$) have $\log(a/b) > 0.7$, therefore we must be aware of possible biases in our results due to dust.

From the findings of Masters et al. (2010) and Buat et al. (2005) above, we estimate the extinction to be $u - r \sim 0.2$ mag and $NUV - u \sim 0.3$ mag, therefore the average change in the SFH parameters across a range of input colours $0 < u - r < 4$ and $-1 < NUV - u < 5$, are $\Delta t_{\rm q} = 0.985$ Gyr, $\Delta\tau = 1.571$ Gyr. This change therefore causes the SFH parameters derived to move towards earlier times and faster quenching rates. Results should be viewed with the caveat, particularly for higher mass, disc galaxies, that earlier values of $t_{\rm q}$ and more rapid values of τ may be inferred by STARPY. However, we note that (i) applying these average corrections across each sample population does not change our main conclusions, (ii) that results are consistent if the population of edge-on and face-on galaxies are compared and (iii) that results do not change if only face-on galaxies are used in the investigation, strongly suggesting that the internal galactic extinction does not systematically bias our results.

SDSS images for 10 randomly selected galaxies from the AGN-HOST sample are shown in Fig. 1; Fig. 2 shows the entire AGN-HOST sample and the matched GZ2-GALEX galaxies on a BPT diagram. For the AGN-HOST sample, the mean $\log(L[{\rm O\,III}]\ [{\rm erg\ s^{-1}}]) \sim 41.3$ and median $\log(L[{\rm O\,III}]\ [{\rm erg\ s^{-1}}]) \sim 41.0$, with a range of $\log(L[{\rm O\,III}]\ [{\rm erg\ s^{-1}}])$ luminosities of 39.4–43.0.

[1] http://zoo2.galaxyzoo.org/

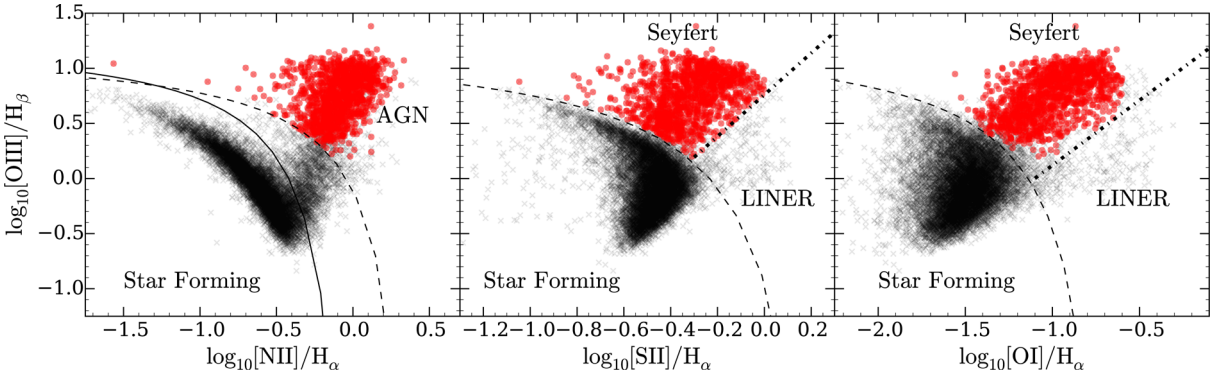

Figure 2. BPT diagrams for galaxies in the GZ2-GALEX sample (black crosses) with S/N > 3 for each emission line. Inequalities defined in: Kewley et al. (2001) to separate SF galaxies from AGN (dashed lines), Kauffman et al. (2003b) to separate SF from composite SF-AGN galaxies (solid line) and Kewley et al. (2006) to separate LINERS and Seyferts (dotted lines). Galaxies are included in the AGN-HOST sample (red circles) if they satisfy all the inequalities to be classified as Seyferts. LINERs are excluded for purity.

We constructed a sample of inactive galaxies by removing from the GZ2-GALEX sample all galaxies with line strengths indicative of potential AGN activity (Kauffman et al. 2003b), as well as sources identified as Type 1 AGN by the presence of broad emission lines (Oh et al. 2015). We select mass- and morphology-matched inactive samples by identifying between 1 and 5 inactive galaxies for each AGN-HOST galaxy with the same stellar mass (to within ±5 per cent) and GZ2 'smooth' and 'disc' vote fractions (to within ±0.1); this selects 6107 galaxies. We refer to this sample as the INACTIVE sample. A Kolmogorov–Smirnov test revealed that the redshift distributions of the INACTIVE and AGN-HOST samples are statistically indistinguishable ($D \sim 0.16$, $p \sim 0.88$).

We show the AGN-HOST and INACTIVE samples on both an optical colour–magnitude diagram and in the star formation rate (SFR)–stellar mass plane in Fig. 3 in comparison to the distribution of SDSS DR7 galaxies. SFRs and stellar masses are obtained from the MPA-JHU catalogue, where available, which follow the prescriptions outlined in Brinchmann et al. (2004) and Salim et al. (2007) for calculating the total aperture corrected galaxy SFR in the presence of an AGN.

We note that the majority of the AGN-HOST sample would be defined as residing in the blue cloud (73 per cent) on the optical colour–magnitude diagram despite the fact that a significant proportion of the sample (47 per cent) lies more than 1σ(0.3dex) below the star-forming 'main sequence' (fit to the MPA-JHU catalogue of SDSS DR7 of Kauffman et al. 2003a; Brinchmann et al. 2004, see Fig. 3).

Ko et al. (2013) show that in a sample of quiescent red sequence galaxies without Hα emission, 26 per cent show NUV excess emission and that the fraction with recent SF is 39 per cent. This is more clearly visible in Fig. 3(b), where a substantial fraction of both the AGN-HOST and INACTIVE samples, all of the sources in which they have detected NUV emission, nevertheless lie more than 1σ below the SF sequence. We do not make a cut on either the AGN-HOST or INACTIVE samples for SFR. The SFH of the entire samples are fitted, however, we describe in Section 2.3 how our method accounts for those galaxies not appropriately fit by a quenching model and downweights their contribution to the final results.

Since this investigation is focused on whether an AGN can have an impact on the SF of its host galaxy, we must also consider possible selection effects. The extent to which SF could obscure AGN emission was addressed by Schawinski et al. (2010). They showed, via analysis of simulated AGN emission added to star-forming galaxies, that BPT-based selection of AGN produces a complete sample at luminosities of $L[\mathrm{O\,III}] > 10^{40}$ erg s^{-1}. Above this limit, we therefore assume that we have selected a complete sample of AGN independent of host galaxy SFR.

2.3 Bayesian SFH determination

STARPY [2] is a PYTHON code which allows the user to derive the quenching SFH of a single galaxy through a Bayesian Markov Chain Monte Carlo method (Foreman-Mackey et al. 2013)[3] with the input of the observed $u - r$ and $NUV - u$ colours, a redshift, and the use of the stellar population models of Bruzual & Charlot (2003). These models are implemented using solar metallicity (varying this does not substantially affect these results; Smethurst et al. 2015) and a Chabrier initial mass function (Chabrier 2003) but does not model for intrinsic dust (see Section 2.2). The SFH is modelled as an exponential decline of the SFR described by two parameters [t_q, τ], where t_q is the time at the onset of quenching [Gyr] and τ is the exponential rate at which quenching occurs [Gyr]. Under the simplifying assumption that all galaxies formed at $t = 0$ Gyr with an initial burst of SF, the SFH can be described as

$$\mathrm{SFR} = \begin{cases} i_{\mathrm{sfr}}(t_q) & \text{if } t < t_q \\ i_{\mathrm{sfr}}(t_q) \times \exp\left(\frac{-(t-t_q)}{\tau}\right) & \text{if } t > t_q \end{cases}, \quad (1)$$

where i_{sfr} is an initial constant SFR dependent on t_q (Schawinski et al. 2014; Smethurst et al. 2015). A smaller τ value corresponds to a rapid quench, whereas a larger τ value corresponds to a slower quench. We note that a galaxy undergoing a slow quench is not necessarily quiescent by the time of observation. Similarly, despite a rapid quenching rate, SF in a galaxy may still be ongoing at very low rates, rather than being fully quenched. This SFH model has previously been shown to appropriately characterize quenching galaxies (Weiner et al. 2006; Martin et al. 2007; Noeske et al. 2007; Schawinski et al. 2014). We note also that star-forming galaxies in this regime are fit by a constant SFR with a $t_q \simeq \mathrm{Age}(z)$, (i.e. the age of the Universe at the galaxy's observed redshift) with a very low probability.

The probabilistic fitting methods to these SFHs for an observed galaxy are described in full detail in section 3.2 of Smethurst et al. (2015), wherein the STARPY code was used to characterize the SFHs of each galaxy in the GZ2-GALEX sample. We assume a flat prior on all the model parameters and the difference between the

[2] Publicly available: http://github.com/zooniverse/starpy
[3] http://dan.iel.fm/emcee/

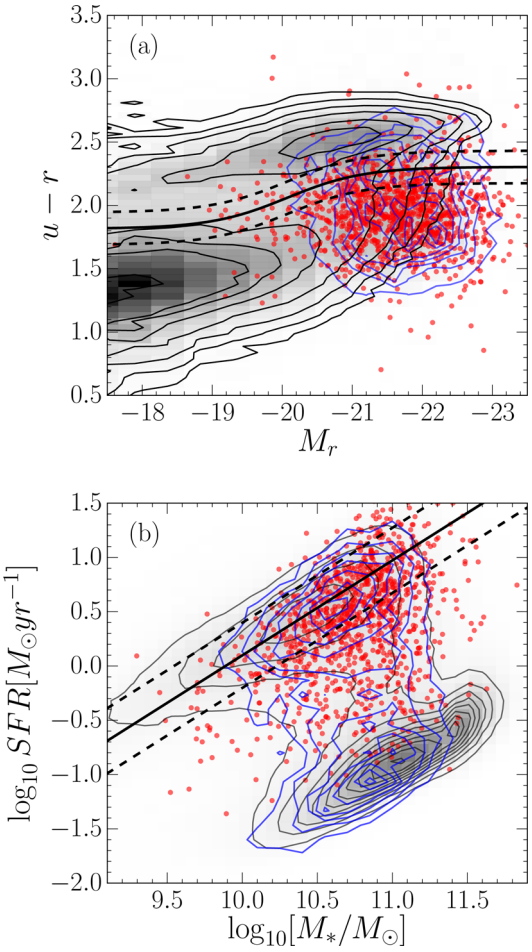

Figure 3. (a) Optical colour–magnitude diagram showing the SDSS DR7 (grey filled contours), the AGN-HOST sample (red circles) and INACTIVE sample (blue contours). The definition of the green valley from Baldry et al. (2006) (solid line) with $\pm 1\sigma$ (dashed lines) is shown. (b) SFR–stellar mass diagram showing the MPA-JHU measurements of SFR and M_* of SDSS DR7 galaxies (Kauffman et al. 2003a; Brinchmann et al. 2004; black contours), the AGN-HOST sample (red circles) and INACTIVE sample (blue contours). The star-forming 'main sequence' fitted by eye to the MPA-JHU catalogue data is shown (solid line) with ± 0.3 dec (dashed lines).

observed and predicted $u-r$ and $NUV-u$ colours are modelled as independent realizations of a double Gaussian likelihood function (equation 2 in Smethurst et al. 2015). We also make the simplifying assumption that the age of each galaxy, $t_{\rm age}$ corresponds to the age of the Universe at its observed redshift, $t_{\rm obs}$.

The output of STARPY is probabilistic in nature and provides the posterior probability distribution across the two-parameter space for an individual galaxy the degeneracies which can be seen in fig. 4 of Smethurst et al. (2015). To study the SFH across a population of galaxies, these individual posterior probability distributions are stacked in $[t, \tau]$ space and weighted by their probability. This is to minimize the contribution of galaxies poorly fit by this exponentially declining SFH, therefore galaxies in each sample which reside on the main sequence will not contribute to the final population distribution of quenching parameters shown in Figs 4 and 5. This is no longer inference but is a method to visualize the results across a population of galaxies. An alternative method would be to perform inference on hierarchical Bayesian parent parameters, $\vec{\theta'}$, to describe the population. Such a hierarchical method, however, requires an initial decision on the functional shape of this parent distribution, which introduces non-trivial assumptions. A discussion of this approach and the decision to use an alternative approach can be found in Section C.

We obtain separate stacked population distributions for both smooth and disc galaxies by using the GZ2 debiased vote fractions for disc ($p_{\rm d}$) or smooth ($p_{\rm s}$) morphologies as weights when stacking, as in Smethurst et al. (2015). This ensures that the entirety of the population is used, with galaxies with a higher $p_{\rm d}$ contributing more to the disc-weighted than the smooth-weighted population density. This negates the need for a threshold on the GZ2 vote fractions (e.g. $p_{\rm d} > 0.8$ as used in Schawinski et al. 2014). These distributions will be referred to as the population densities.

We also split both the AGN-HOST and INACTIVE samples into low-, medium- and high-mass ranges (see Table 1) to investigate any trends in the SFH with mass. The mass boundaries were chosen to give roughly equal numbers of inactive galaxies in each bin prior to the mass matching to the AGN-HOST sample.

3 RESULTS

Figs 4 and 5 show the stacked population density distributions for the quenching time, $t_{\rm q}$, and exponential quenching rate, τ, respectively. In each figure, the population density, along with shaded regions to show the uncertainties, for a given parameter is shown for smooth and disc galaxy populations across three mass bins for the AGN-HOST and INACTIVE samples. No cut on the SFR is made to the galaxies which contribute to Figs 4 and 5, but those galaxies poorly fit by an exponentially declining SFH are downweighted so that they do not contribute to the results presented here. In Table 1, the percentage of the population density in each quenching regime for rapid ($\tau < 1$ Gyr), intermediate ($1 < \tau$ [Gyr] < 2) and slow ($\tau > 2$ Gyr) quenching time-scales, are shown. Uncertainties on the population densities (shown by the shaded regions) are determined from the maximum and minimum values spanned by $N = 1000$ bootstrap iterations, each sampling 90 per cent of the galaxy population. 1σ uncertainties are quoted for the percentages in Table 1, calculated from the bootstrapped distributions.

These population densities should be interpreted as the spread of quenching times and rates occurring in galaxies which have either undergone or are undergoing quenching within a population. Figs 4 and 5 show a distinct difference between the population density of AGN-HOST and INACTIVE quenching parameters.

At all masses, the population density for galaxies within the AGN-HOST population across the quenching time $t_{\rm q}$ parameter (left-hand panels of Fig. 4) is different from that of the inactive galaxies (right-hand panels of Fig. 4). Recent quenching ($t > 11$ Gyr) is the dominant history for quenched and quenching low- and medium-mass AGN-HOST galaxies, particularly for the smooth galaxies hosting an AGN. However, this effect is less dominant in higher mass galaxies where quenching at earlier times also has high density.

The population densities for the quenching rate, τ, in Fig. 5 and Table 1, show the dominance of rapid quenching ($\tau < 1$ Gyr) within the AGN-HOST population, particularly for smooth galaxies. With increasing mass, the dominant quenching rate becomes slow ($\tau > 2$ Gyr), especially for disc galaxies hosting an AGN. Similar trends in the density are observed within the INACTIVE population but the overall distribution is very different.

The distributions for the AGN-HOST galaxies therefore show evidence for the dominance of rapid, recent quenching within this population. This result implies the importance of AGN feedback for the evolution of these galaxies.

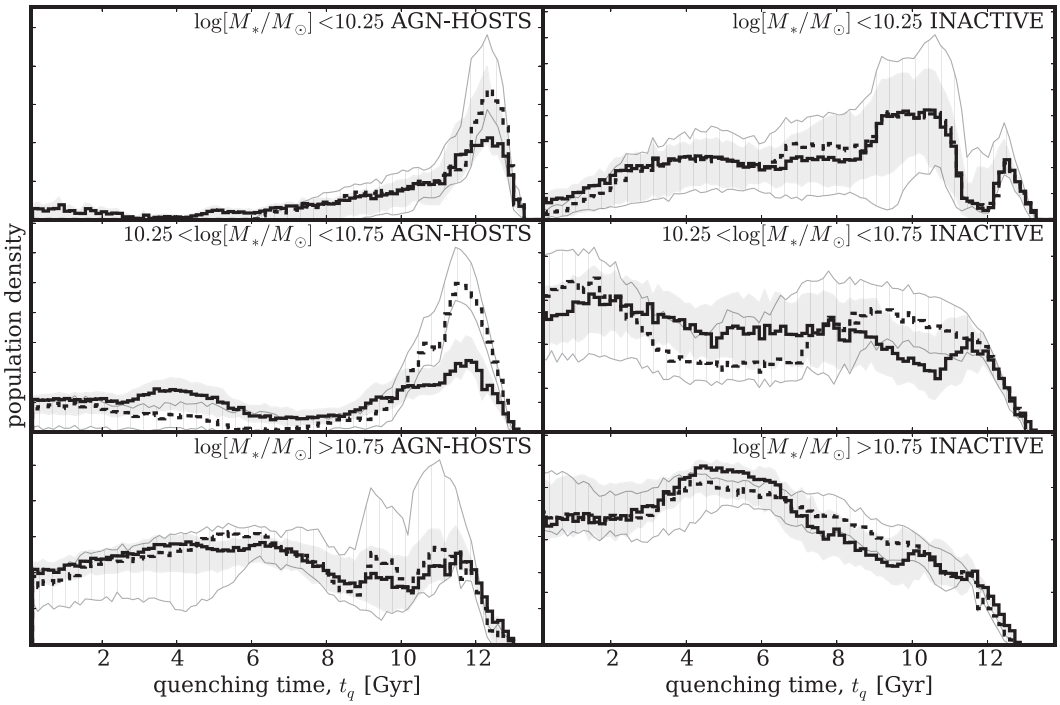

Figure 4. Population density distributions for the quenching time (t_q) parameter, normalized so that the areas under the curves are equal. AGN-HOST (left) and INACTIVE (right) galaxies are split into low (top), medium (middle) and high (bottom) mass for smooth (dashed) and disc (solid) galaxies. Uncertainties from bootstrapping are shown by the shaded regions for the smooth (grey striped) and disc (grey solid) population densities. A low (high) value of t_q corresponds to the early (recent) Universe.

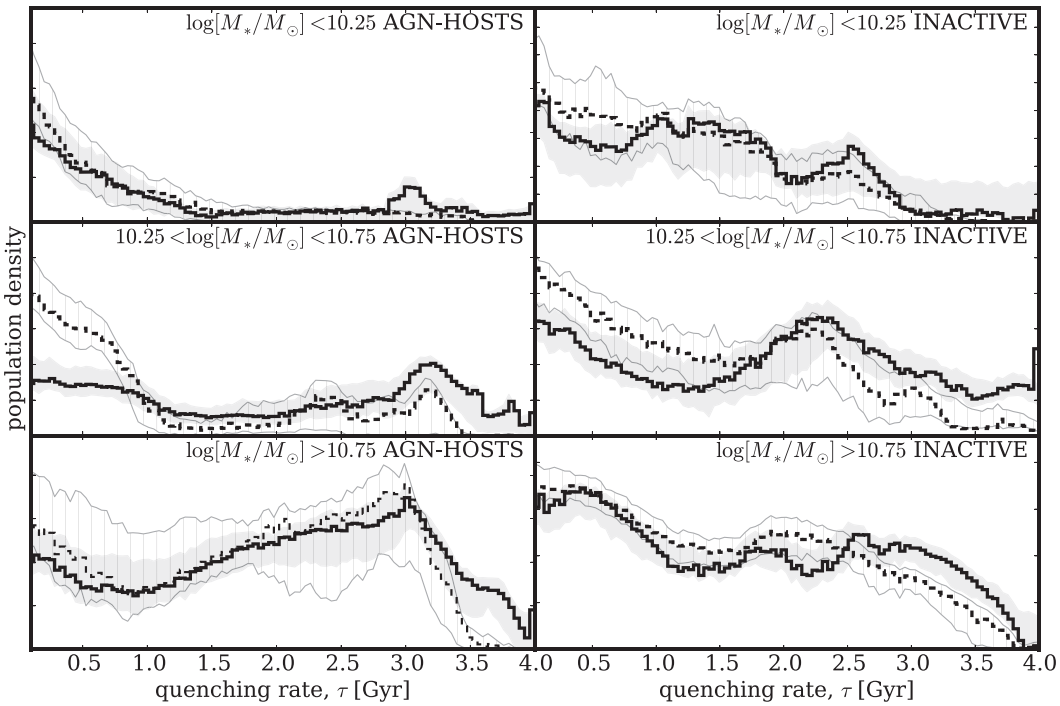

Figure 5. Population density distributions for the quenching rate (τ) normalized so that the areas under the curves are equal. AGN-HOST (left) host and INACTIVE (right) galaxies are split into low (top), medium (middle) and high (bottom) mass for smooth (dashed) and disc (solid) galaxies. Uncertainties from bootstrapping are shown by the shaded regions for the smooth (grey striped) and disc (grey solid) population densities. A small (large) value of τ corresponds to a rapid (slow) quench.

Table 1. Table showing the number of galaxies in each of the three mass bins for both the AGN-HOSTS and INACTIVE galaxy samples and the percentage of the distribution across each morphologically weighted population found in the rapid, intermediate and slow quenching regimes.

Sample	Mass bin	Weighting	$\tau < 1$ (Gyr)	$1 < \tau$ (Gyr) < 2	$\tau > 2$ (Gyr)	Number
	$\log[M_*/\mathrm{M}_\odot] < 10.25$	p_d	$60\pm^{23}_{5}$	$13\pm^{9}_{9}$	$28\pm^{6}_{19}$	165(13.3 per cent)
		p_s	$69\pm^{14}_{6}$	$17\pm^{6}_{14}$	$14\pm^{3}_{7}$	
AGN-HOSTS	$10.25 < \log[M_*/\mathrm{M}_\odot] < 10.75$	p_d	$33\pm^{3}_{5}$	$15\pm^{4}_{4}$	$51\pm^{4}_{7}$	630(50.6 per cent)
		p_s	$69\pm^{4}_{5}$	$7\pm^{4}_{4}$	$26\pm^{5}_{9}$	
	$\log[M_*/\mathrm{M}_\odot] > 10.75$	p_d	$20\pm^{5}_{4}$	$25\pm^{7}_{5}$	$56\pm^{8}_{12}$	449(36.1 per cent)
		p_s	$24\pm^{4}_{3}$	$26\pm^{5}_{6}$	$50\pm^{7}_{7}$	
	$\log[M_*/\mathrm{M}_\odot] < 10.25$	p_d	$37\pm^{8}_{14}$	$39\pm^{8}_{6}$	$24\pm^{8}_{6}$	807(13.2 per cent)
		p_s	$47\pm^{5}_{11}$	$36\pm^{9}_{5}$	$17\pm^{4}_{5}$	
INACTIVE	$10.25 < \log[M_*/\mathrm{M}_\odot] < 10.75$	p_d	$30\pm^{4}_{3}$	$18\pm^{2}_{3}$	$51\pm^{4}_{4}$	3094(50.7 per cent)
		p_s	$42\pm^{2}_{2}$	$29\pm^{3}_{3}$	$30\pm^{3}_{4}$	
	$\log[M_*/\mathrm{M}_\odot] > 10.75$	p_d	$36\pm^{3}_{3}$	$24\pm^{3}_{4}$	$41\pm^{4}_{3}$	2206(36.1 per cent)
		p_s	$38\pm^{2}_{2}$	$28\pm^{3}_{4}$	$34\pm^{3}_{3}$	

4 DISCUSSION

The differences between the population density distributions of the AGN-HOST and INACTIVE populations reveal that an AGN can have a significant effect on the SFH of its host galaxy. Both recent, rapid quenching and early, slow quenching are observed in the population density within the AGN-HOST population.

There are minimal differences between the smooth- and disc-weighted distributions of the quenching parameters within the AGN-HOST population. This is in agreement with the conclusions of Kauffman et al. (2003b) who found that the structural properties of AGN hosts depend very little on AGN power.

The difference between the AGN-HOST and INACTIVE population distributions in Fig. 5 for the rate of quenching, τ, tells a story of gas reservoirs. The density distribution for higher mass AGN-HOST galaxies is dominated by slow, early quenching implying that another mechanism is responsible for the cessation of SF within a proportion of these high-mass galaxies prior to the triggering of the current AGN. This preference for slow evolution time-scales follows from the ideas of previously isolated discs evolving slowly by the Kennicutt–Schmidt (Schmidt 1959; Kennicutt 1997) law which can then undergo an interaction or merger to reinvigorate SF, feed the central black hole and trigger an AGN (Varela et al. 2004; Emsellem et al. 2015). These galaxies would need a large enough gas reservoir to fuel both SF throughout their lifetimes and the recent AGN. These high-mass galaxies also play host to the most luminous AGN (mean $\log(L[\mathrm{O\,III}]\ [\mathrm{erg\ s^{-1}}]) \sim 41.6$) and so this SFH challenges the usual explanation for the co-evolution of luminous black holes and their host galaxies driven by merger growth.

Quenching at early times is also observed within a subsample of the INACTIVE population, where the density for the quenching time is roughly constant until recent times where the distribution drops off. This drop-off occurs at earlier times with increasing mass with a significant lack of quenching occurring at early times for low-mass INACTIVE galaxies (right-hand panels, Fig. 4). This is evidence of downsizing within the INACTIVE galaxy population, whereby stars in massive galaxies form first and quench early (Cowie et al. 1996; Thomas et al. 2010).

Some of the most massive AGN-HOST galaxies also show a preference for earlier quenching (bottom-left panel, Fig. 4) occurring at slow rates; we speculate that this is also due to the effects of downsizing rather than being caused by the current AGN. This earlier evolution would first form a slowly 'dying' or 'dead' galaxy typical of massive elliptical galaxies which can then have a recent infall of gas either through a minor merger, galaxy interaction or environmental change, triggering further SF and feeding the central black hole, triggering an AGN (Kaviraj 2014). In turn, this AGN can then quench the recent boost in SF. This track is similar to the evolution history proposed for blue ellipticals (Kaviraj et al. 2013; McIntosh et al. 2014; Haines et al. 2015). This SFH would then give rise to the distribution seen within the high-mass AGN-HOST population for both time and rate parameters.

These recently triggered AGN in both massive disc and smooth galaxies do not have the ability to impact the SF across the entirety of a high-mass galaxy in a deep gravitational potential (Ishibashi & Fabian 2012; Zinn et al. 2013). This leads to the lower peak for recent, rapid quenching within the high-mass AGN-HOST population for both morphologies.

Conversely, rapid quenching, possibly caused by the AGN itself through negative feedback, is the most dominant history within the low-mass AGN-HOST population with lower gravitational potentials from which gas may be more readily expelled or heated (Tortora et al. 2009).

Tortora et al. (2009) model the effects of jet-induced AGN feedback on a typical early-type (i.e. smooth) galaxy and observe a drastic suppression of SF on a time-scale of ~3 Myr. Comparing their synthetic colours with observed colours of SDSS elliptical galaxies, they find that the time between the current galaxy age, t_gal, and the time that the feedback began, t_AGN, peaks at $t_\mathrm{gal} - t_\mathrm{AGN} \sim 0.85$ Gyr. This agrees with the location of the peak in Fig. 4 for low-mass galaxies which have undergone quenching, where the difference between the peak of the distribution and the average age of the population (galaxy age is calculated as the age of the Universe at the observed redshift, by assuming all galaxies form at $t = 0$) is ~0.83 Gyr. This implies that this SFH dominated by recent quenching is caused directly by negative AGN feedback.

However, there still remains the possibility that the AGN is merely a consequence of an alternative quenching mechanism. This idea is supported by simulations showing that the exhaustion of gas by a merger fuelled starburst could cause such a rapid quench in SF and in turn also trigger an AGN (Croton et al. 2006; Wild et al. 2009; Snyder et al. 2011; Hayward et al. 2014). Yesuf et al. (2014) also showed that AGN are more commonly hosted by post-starburst galaxies, with the peak AGN activity appearing

$\geq 200 \pm 100$ Myr after the starburst. Such an SFH is not accounted for in the models presented here, however, this scenario is still consistent with the results presented in this paper; that AGN which are currently active have been detected in host galaxies $\sim$1 Gyr after the onset of quenching.

This rapid quenching is particularly dominant for low-to-medium mass smooth galaxies. Smethurst et al. (2015) suggest that incredibly rapid quenching rates could be attributed to mergers of galaxies in conjunction with AGN feedback, which are thought to be responsible for creating the most massive smooth galaxies (Conselice et al. 2003; Springel, Di Matteo & Hernquist 2005; Hopkins et al. 2008). This dominance of rapid quenching across the smooth AGN-HOST population supports the idea that a merger, having caused a morphological transformation to a smooth galaxy, can also trigger an AGN, causing feedback and cessation of SF (Sanders et al. 1988).

Within the medium-mass AGN-HOST population, we see a bimodal distribution between these two quenching histories, highlighting the strength of this method which is capable of detecting such variation in the SFHs within a population of galaxies.

Indeed not all galaxies in the AGN-HOST and INACTIVE samples are quenching, as seen in Fig. 3, with a significant proportion of both the AGN-HOST and INACTIVE samples lying on the star-forming sequence. A galaxy can therefore still maintain SF whilst hosting an AGN. The results presented in Section 3 only reflect the trends for galaxies that have undergone or are currently undergoing quenching within a population and can therefore be accurately fit by an exponentially declining SFH. This prevalence of star-forming AGN host galaxies, combined with the results above allows us to consider that either: (i) the AGN are the cause of the rapid quenching observed but only in gas-poor host galaxies where they can have a large impact, (ii) the AGN are a consequence of another quenching mechanism but can also be triggered by other means which do not cause quenching, or (iii) the SFR of a galaxy can recover post-quench and return to the star-forming sequence after a few Gyr (see recent simulations by Pontzen et al. 2016). Further investigation will therefore be required to determine the nature of this quenching.

We have used morphological classifications from the Galaxy Zoo 2 project to determine the morphology-dependent SFHs of a population of 1244 Type 2 Seyfert AGN host galaxies, in comparison to an inactive galaxy population, via a partially Bayesian analysis of an exponentially declining SFH model. We determined the population distribution for the quenching onset time, t_q, and exponential quenching rate, τ, and find clear differences in the distributions, between inactive and AGN host galaxy populations. We have demonstrated a clear dependence on a galaxy currently hosting an AGN and its SFH for those galaxies which have undergone or are undergoing quenching. There is strong evidence for downsizing in massive inactive galaxies, which appears as a secondary effect in AGN host galaxies. The dominant mechanism for quenched and quenching galaxies currently hosting an AGN is for rapid quenching which has occurred very recently. This result demonstrates the importance of AGN feedback within the host galaxy population, in driving the evolution of galaxies across the colour–magnitude diagram.

ACKNOWLEDGEMENTS

The authors would like to thank S. Kaviraj and P. Marshall for helpful discussions. We also thank both of the anonymous referees for helpful comments that greatly improved the clarity of the paper.

RJS acknowledges funding from the STFC Grant Code ST/K502236/1. BDS gratefully acknowledges support from Balliol College, Oxford. KS gratefully acknowledges support from Swiss National Science Foundation Grant PP00P2 138979/1. SJK acknowledges funding from the STFC Grant Code ST/MJ0371X/1. KLM acknowledges funding from The Leverhulme Trust as a 2010 Early Career Fellow. KWW acknowledges funding from NSF grant AST-1413610. OIW acknowledges a Super Science Fellowship from the Australian Research Council. Support for this work was provided by the National Aeronautics and Space Administration through Einstein Postdoctoral Fellowship Award Number PF5-160143 issued by the Chandra X-ray Observatory Center, which is operated by the Smithsonian Astrophysical Observatory for and on behalf of the National Aeronautics Space Administration under contract NAS8-03060. The development of Galaxy Zoo was supported by the Alfred P. Sloan Foundation and The Leverhulme Trust. Based on observations made with the NASA *GALEX*[4] and the SDSS.[5]

REFERENCES

Abazajian K. N. et al., 2009, ApJS, 182, 543
Baldry I., Balogh M. L., Bower R. G., Glazebrook K., Nichol R. C., Bamford S. P., Budavari T., 2006, MNRAS, 373, 469
Baldwin J. A., Phillips M. M., Terlevich R., 1981, PASP, 93, 5
Blanton M. R., Roweis S., 2007, AJ, 133, 734
Blanton M. R. et al., 2005, AJ, 129, 2562
Bower R., Benson A. J., Malbon R., Helly J. C., Frenk C. S., Baugh C. M., Cole S., Lacey C. G., 2006, MNRAS, 370, 645
Brinchmann J., Charlot S., White S. D. M., Tremonti C., Kauffmann G., Heckman T., Brinkmann J., 2004, MNRAS, 351, 1151
Bruzual G., Charlot S., 2003, MNRAS, 344, 1000
Buat V. et al., 2005, ApJ, 619, 51
Cardelli J. A., Clayton G. C., Mathis J. S., 1989, ApJ, 345, 245
Chabrier G., 2003, ApJ, 586, L133
Conselice C. J., Bershady M. A., Dickinson M., Papovich C., 2003, AJ, 126, 1183
Cowie L., Barger A. J., 2008, ApJ, 686, 72
Cowie L., Songaila A., Hu E. M., Cohen J. G., 1996, AJ, 112, 839
Croton D. J. et al., 2006, MNRAS, 365, 11
Emsellem E., Renaud F., Bournaud F., Elmegreen B., Combes F., Gabor J. M., 2015, MNRAS, 446, 2468
Fabian A. C., 2006, ARA&A, 50, 455
Foreman-Mackey D., Hogg D. W., Lang D., Goodman J., 2013, PASP, 125, 306
Haines T., McIntosh D. H., Sánchez S. F., Tremonti C., Rudnick G., 2015, MNRAS, 451, 433
Haring N., Rix H.-W., 2004, ApJ, 604, 89
Hayward C. C., Torrey P., Springel V., Hernquist L., Vogelsberger M., 2014, MNRAS, 442, 1992
Hickox R. C. et al., 2009, ApJ, 696, 891
Hopkins F., Cox T. J., Kereš D., Hernquist L., 2008, ApJSS, 175, 390
Ishibashi W., Fabian A. C., 2012, MNRAS, 427, 2998
Jarosik N. et al., 2011, ApJS, 192, 14
Kauffman G. et al., 2003a, MNRAS, 341, 33
Kauffman G. et al., 2003b, MNRAS, 346, 1055
Kaviraj S. et al., 2013, MNRAS, 428, 925
Kaviraj S., 2014, MNRAS, 440, 2944
Kennicutt R. C., 1997, ApJ, 498, 491
Kewley L. J., Dopita M. A., Sutherland R. S., Heisler C. A., Trevena J., 2001, ApJ, 556, 121

[4] http://galex.stsci.edu/GR6/
[5] https://www.sdss3.org/collaboration/boiler-plate.php

Kewley L. J., Groves B. Kauffmann G. Heckman T., 2006, MNRAS, 372, 961
Ko J., Hwang H. S., Lee J. C., Sohn Y.-J., 2013, ApJ, 767, 90
Lahav O., Bridle S. L., Hobson M. P., Lasenby A. N., Sodré L., 2000, MNRAS 315, L45
McIntosh D. et al., 2014, MNRAS, 442, 533
MacKay D. J. C., 2003, Information Theory, Inference and Learning Algorithms. Cambridge Univ. Press, Cambridge
Magorrian J. et al., 1998, AJ, 115, 2285
Marconi A., Hunt L. K., 2003, ApJ, 589, 21
Martin D. C. et al., 2005, ApJ, 619, L1
Martin D. C. et al., 2007, ApJSS, 173, 342
Masters K. et al., 2010, MNRAS, 404, 792
Noeske K. G. et al., 2007, ApJ, 660, L47
Oh K., Sarzi M., Schawinski K., Yi S. K., 2011, ApJS, 195, 13
Oh K., Yi S. K., Schawinski K., Koss M., Trakhtenbrot B., Soto K., 2015, ApJS, 219, 1
Padmanabhan N. et al., 2008, ApJ, 674, 121
Pontzen A., Tremmel M., Roth N., Peiris H. V., Saintonge A., Volonteri M., Quinn T., Governato F., 2016, preprint (arXiv:1607.02507)
Salim S. et al., 2007, ApJSS, 173, 267
Sanders D. B. Soifer B. T., Elias J. H., Madore B. F., Matthews K., Neugebauer G., Scoville N. Z., 1988, ApJ, 325, 74
Sarzi M. et al., 2010, MNRAS, 402, 2187
Schawinski K. et al., 2010, MNRAS, 711, 284
Schawinski K. et al., 2014, MNRAS, 440, 889
Schmidt M., 1959, ApJ, 129, 243
Silk J., Rees M. J., 1998, A&A, 331, L1
Simmons B. D., Van Duyne J., Urry C. M., Treister E., Koekemoer A. M., Grogin N. A., GOODS Team, 2011, ApJ, 734, 121
Singh R. et al., 2013, A&A, 558, 43
Smethurst R. J. et al., 2015, MNRAS, 450, 435
Snyder G. F., Cox T. J., Hayward C. C., Hernquist L., Jonsson P., 2011, ApJ, 741, 77
Somerville R. S., Hopkins P. F., Cox T. J., Robertson B. E., Hernquist L., 2008, MNRAS, 391, 481
Springel V., Di Matteo T., Hernquist L., 2005, ApJ, 620, L79
Thomas D., Maraston C., Schawinski K., Sarzi M., Silk J., 2010, MNRAS, 404, 1775
Tortora C., Antonuccio-Delogu V., Kaviraj S., Silk J., Romeo A. D., Becciani U., 2009, MNRAS, 369, 61
Varela J., Moles M., Márquez I., Galletta G., Masegosa J., Bettoni D., 2004, A&A, 420, 873
Weiner B. J. et al., 2006, ApJ, 653, 1049
Wild V., Walcher C. J., Johansson P. H., Tresse L., Charlot S., Pollo A., Le Fèvre O., de Ravel L., 2009, MNRAS, 395, 144
Willett K. et al., 2013, MNRAS, 435, 2835
Yan R., Blanton M. R., 2012, ApJ, 747, 61
Yesuf H. M., Faber S. M., Trump J. R., Koo D. C., Fang J. J., Liu F. S., Wild V., Hayward C. C., 2014, ApJ, 792, 84
York D. G. et al., 2000, AJ, 120, 1579
Zinn P., Middelberg E., Norris R. P., Dettmar R.-J., 2013, ApJ, 774, 66

APPENDIX A: MASS MATCHED INACTIVE SAMPLE

Each galaxy in the AGN-HOST sample has been matched to at least one and up to five inactive galaxies. These were matched to within ±5 per cent of the stellar mass and ±0.1 of each of the disc and smooth GZ2 vote fractions, p_d and p_s.

Both the AGN-HOST and INACTIVE galaxy samples are shown on an optical-NUV colour–colour diagram in Fig. A1. The INACTIVE sample across all mass bins can be seen to encompass the entirety of the colour–magnitude diagram, unlike the AGN-HOST sample which resides at increasingly green colours with increasing mass.

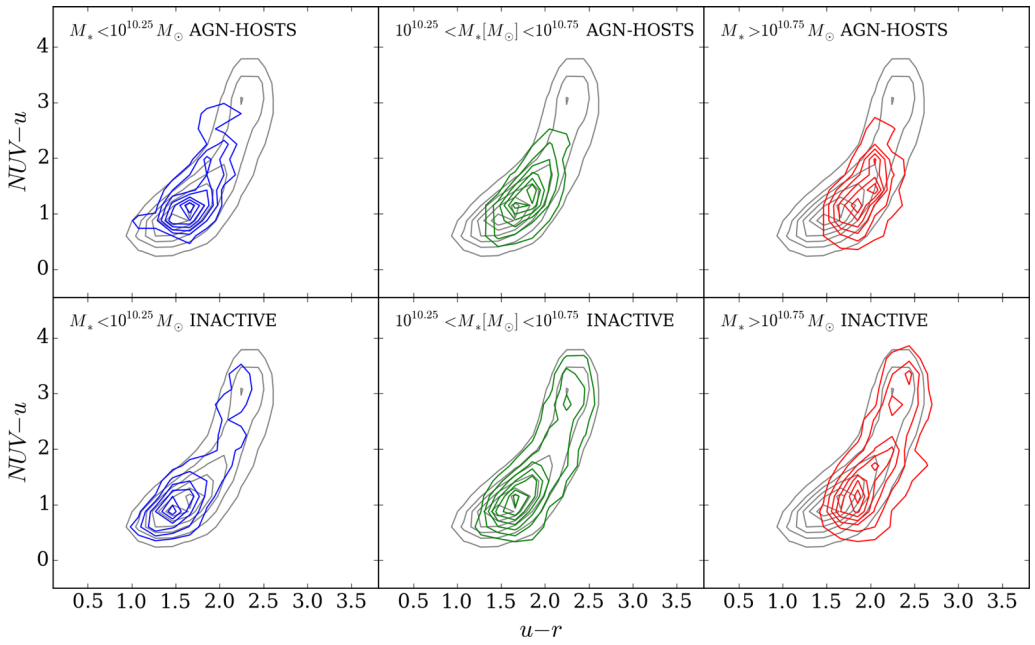

Figure A1. Optical-NUV colour–colour contour diagrams for the AGN-HOST (top) and INACTIVE galaxy samples split into low (blue), medium (green) and high (red) stellar mass samples. Underlaying each diagram are the contours of the GZ2-GALEX sample (grey).

APPENDIX B: LUMINOSITY DEPENDENCE

An investigation into the dependence of the quenching in the AGN-HOST sample with L[O III] was also conducted, with the summed weighted population density distributions for the quenching time and rate parameters shown in Figs B1 and B2. The AGN-HOST sample was split into low, medium and high luminosity as with the stellar mass. Since the L[O III] of the black hole is correlated to the accretion rate (Kauffman et al. 2003b), which is dependent on the black hole mass, which is, in turn, correlated to the mass of the host galaxy (Magorrian et al. 1998), the stellar mass was used in the main investigation to allow us a direct comparison to the control INACTIVE sample.

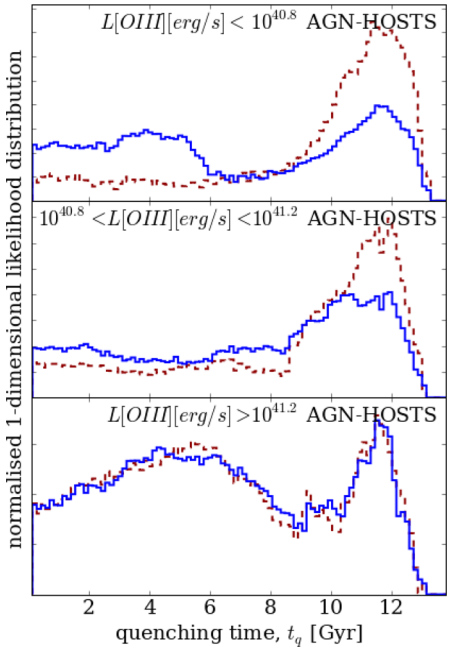

Figure B1. Population density distributions for the quenching time, t_q, normalized, so that the areas under the curves are equal. AGN-HOST galaxies are split into low (top), medium (middle) and high (bottom) L[O III] for smooth (red dashed) and disc (blue solid) galaxies. A low (high) value of t_q corresponds to the early (recent) Universe.

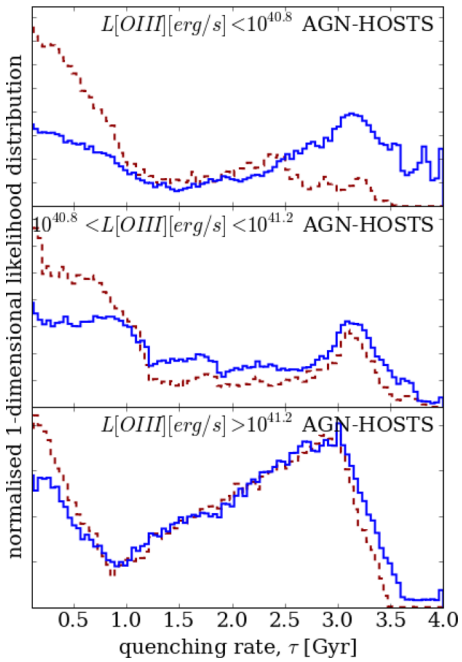

Figure B2. Population density distributions for the quenching rate, τ, normalized, so that the areas under the curves are equal. AGN-HOST galaxies are split into low (top), medium (middle) and high (bottom) L[O III] for smooth (red dashed) and disc (blue solid) galaxies. A small (large) value of τ corresponds to a rapid (slow) quench.

APPENDIX C: ALTERNATIVE HIERARCHICAL BAYESIAN APPROACH

The approach used in the paper to present the main results shown in Figs 4 and 5, relied upon a visualization of the SFHs across each population, with no inference involved beyond the use of STARPY to derive the individual galaxy SFHs. The preferred approach to this problem would be to use a hierarchical Bayesian method to determine the 'hyper-parameters' that describe the distribution of the parent population $\theta' = [t'_q, \tau']$ that each individual galaxy's SFH is drawn from.

We want the posterior PDF for $\vec{\theta}'$ to describe a galaxy population:

$$P(\vec{\theta}'|\boldsymbol{d}) = \frac{P(\boldsymbol{d}|\vec{\theta}')P(\vec{\theta}')}{P(\boldsymbol{d})}, \tag{C1}$$

where $\boldsymbol{d}$ represents all of the optical and NUV colour data in a population $\{\boldsymbol{d}_k\}$. For one galaxy, k, the marginalized likelihood is

$$P(d_k|\vec{\theta}') = \iint P(d_k|t_k, \tau_k)P(t_k, \tau_k|\vec{\theta}')\, \mathrm{d}t_k\, \mathrm{d}\tau_k \tag{C2}$$

and for all galaxies, N, therefore:

$$P(\boldsymbol{d}|\vec{\theta}') = \prod_k^N P(d_k|\vec{\theta}'). \tag{C3}$$

Using STARPY for individual galaxies, we sample from the 'interim' posterior $P(t_k, \tau_k|d_k)$ which we can relate to $P(d_k|t_k, \tau_k)$, so that:

$$P(d_k|\vec{\theta}') = \iint P(t_k, \tau_k|d_k) \cdot\ P(d_k) \cdot \frac{P(t_k, \tau_k|\vec{\theta}')}{P(t_k, \tau_k)}\, \mathrm{d}t_k\, \mathrm{d}\tau_k. \tag{C4}$$

In order to calculate this, we draw N_s random samples, r, from the interim posterior, $P(t_k, \tau_k|d_k)$, so that equation (C4) can be expressed as a sum over a number of random samples, N_s (as with the calculation of an expected mean):

$$P(d_k|\vec{\theta}') = \frac{P(d_k)}{N_s} \sum_r^{N_s} \frac{P(t_{k,r}, \tau_{k,r}|\vec{\theta}')}{P(t_k, \tau_k)}, \tag{C5}$$

for the rth sample of N_s total samples taken from one galaxy's, k, interim posterior PDF. This fraction is known as the 'importance weight', w_r, in importance sampling.

However, we also have two morphological vote fractions that we can weight by to determine separate hyper-parameters, $\vec{\theta}' = [\vec{\theta}'_d, \vec{\theta}'_s]$, for both disc, d, and smooth, s, galaxies. Therefore:

$$w_r = \frac{P(t_{k,r}, \tau_{k,r}|\vec{\theta}')}{P(t_k, \tau_k)} = \frac{p_{d,k}P(t_{k,r}, \tau_{k,r}|\vec{\theta}'_d) + p_{s,k}P(t_{k,r}, \tau_{k,r}|\vec{\theta}'_s)}{P(t_k, \tau_k)}. \tag{C6}$$

If we substitute equation (C5) into equation (C1), we find that the $P(d_k)$ terms cancel and we are left with:

$$P(\vec{\theta}'|\boldsymbol{d}) = P(\vec{\theta}') \prod_k^N \frac{1}{N_{s,k}} \sum_r^{N_s} w_r, \tag{C7}$$

where $P(\vec{\theta}')$ is the assumed prior on the hyper-parameters, which is assumed to be uniform.

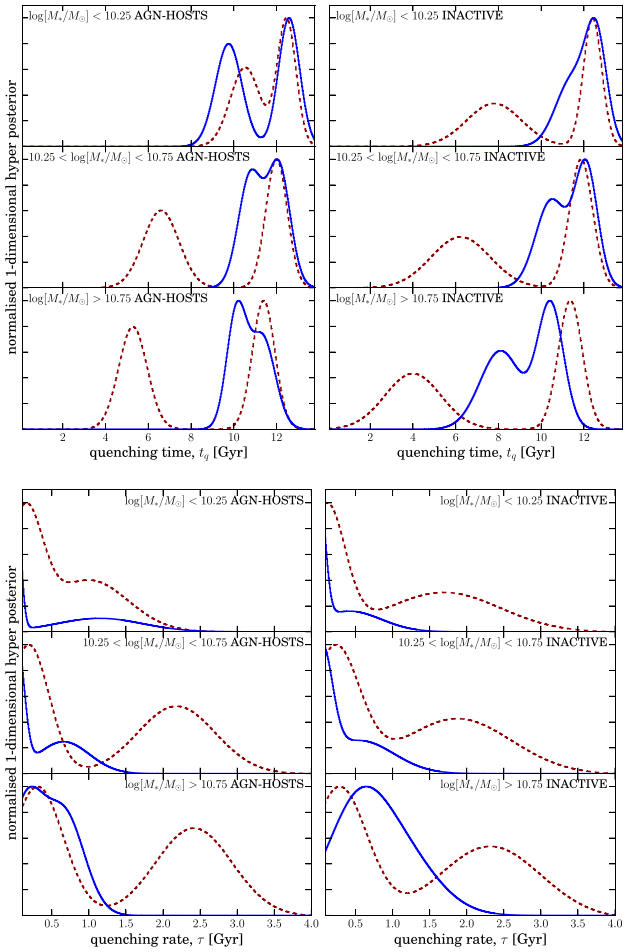

Figure C1. Hierarchical-posterior PDF of the quenching time (t'_q, top) and rate (τ', bottom) population parameters normalized so that the areas under the curves are equal. AGN-HOST (left) and INACTIVE (right) galaxies are split into low (top), medium (middle) and high (bottom) mass, weighted for smooth (red dashed) and disc (blue solid) galaxies. A low (high) value of t'_q corresponds to the early (recent) Universe. A small (large) value of τ' corresponds to a rapid (slow) quench.

This approach is heavily dependent on what shape is assumed for the hyper-distribution; a decision which is not trivial. It is often common for this function to take the form of a multicomponent Gaussian mixture model (Lahav et al. 2000; MacKay 2003). For example, a two-component Gaussian mixture model in $[t, \tau]$ space is described by eight hyper-parameters for a single morphology, $\vec{\theta}' = [\mu_{t,1}, \sigma_{t,1}, \mu_{\tau,1}, \sigma_{\tau,1}, \mu_{t,2}, \sigma_{t,2}, \mu_{\tau,2}, \sigma_{\tau,2}]$. Here, we also assume no covariance between hyper-parameters for simplicity.

We used this assumption of a two-component Gaussian mixture model, to infer the population parameters for both the AGN-HOST and INACTIVE populations and the results are shown in Fig. C1. These results were produced by drawing $N_s = 100$ random samples from each galaxy, k, in each mass bin. We plot the distributions for a given morphology by taking the median value of the posterior distribution for each of the eight parameters describing the two-component Gaussian mixture. We can see in Fig. C1 that this hierarchical method produces similar distributions for the AGN-HOST and INACTIVE samples. This finding is not expected given the differences between the two samples in colour–colour space seen in Fig. A1.

In order to test whether this assumption of a multicomponent Gaussian mixture model is appropriate, we sampled the inferred hierarchical distributions to produce replica data sets in optical-NUV colour space. These are shown here in Fig. C2 in comparison to the observed colour–colour distributions of the AGN-HOST and INACTIVE samples. For all masses and morphologies, the replicated $u - r$ and $NUV - u$ colours do not accurately match the observed data.

We also varied the value of N_s and found that increasing the number of samples drawn did not improve this fit for either the AGN-HOST or INACTIVE populations. Similarly, increasing the number of components in the Gaussian mixture model did not immediately improve the accuracy of the fit. We therefore concluded that this functional form of the population distribution was unsatisfactory. An extensive exploration of a wide variety of functional forms is necessary to ensure the correct conclusions are drawn from the data. Such an investigation is beyond the scope of this paper.

The approach presented in the paper was motivated by the investigation increasing the number of samples, N_s, drawn from the posterior of each galaxy, k, until the point where all the samples were drawn. Instead of attempting to infer parameters to describe this distribution, as above, we presented the distribution itself. The distributions produced by this visualization method, shown in Figs 4 and 5, reveal the complexity that the parent distribution must describe, which, as we concluded earlier, cannot be effectively modelled.

We also tested whether this method is reasonable by producing replica data sets in optical-NUV colour space, as before, by drawing 1000 $[t, \tau]$ values from the unweighted summed distributions presented in Figs 4 and 5. These replica data sets are shown here in Fig. C3 in comparison to the observed colour–colour distributions of the AGN-HOST and INACTIVE samples. Comparing these replica colours in Fig. C3, with those produced by drawing from the inferred hierarchical distributions, shown in Fig. C2, we can see that they produce a more accurate match to the observed data for the majority of masses and morphologies.

We therefore use this visualization method to display the parent population distribution, rather than quoting inferred values to describe it.

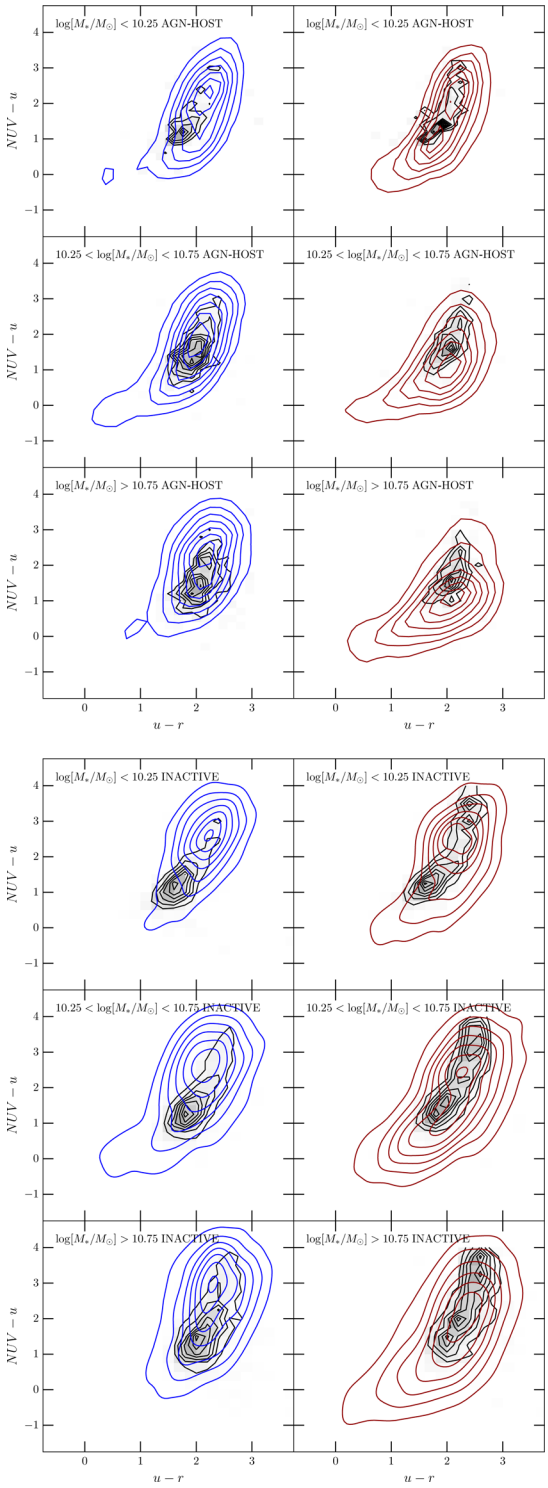

Figure C2. Optical-NUV colour–colour diagrams for the AGN-HOST (top) and INACTIVE (bottom) galaxies shown by the black contours, split into low-mass (top), medium-mass (middle) and high-mass (bottom) galaxies weighted by p_d (left) and p_s (right). Kernel smoothing has been applied to the overlaid replica data sets, which are created by sampling from the inferred 2 component Gaussian mixture model hierarchical parent distributions, shown here in Fig. C1. Gaussian random noise is also added to the inferred colours, with a mean and standard deviation of the errors on the observed colours of the respective sample. Contours are shown for samples taken from the disc (blue) and smooth-weighted (red) inferred hierarchical distributions.

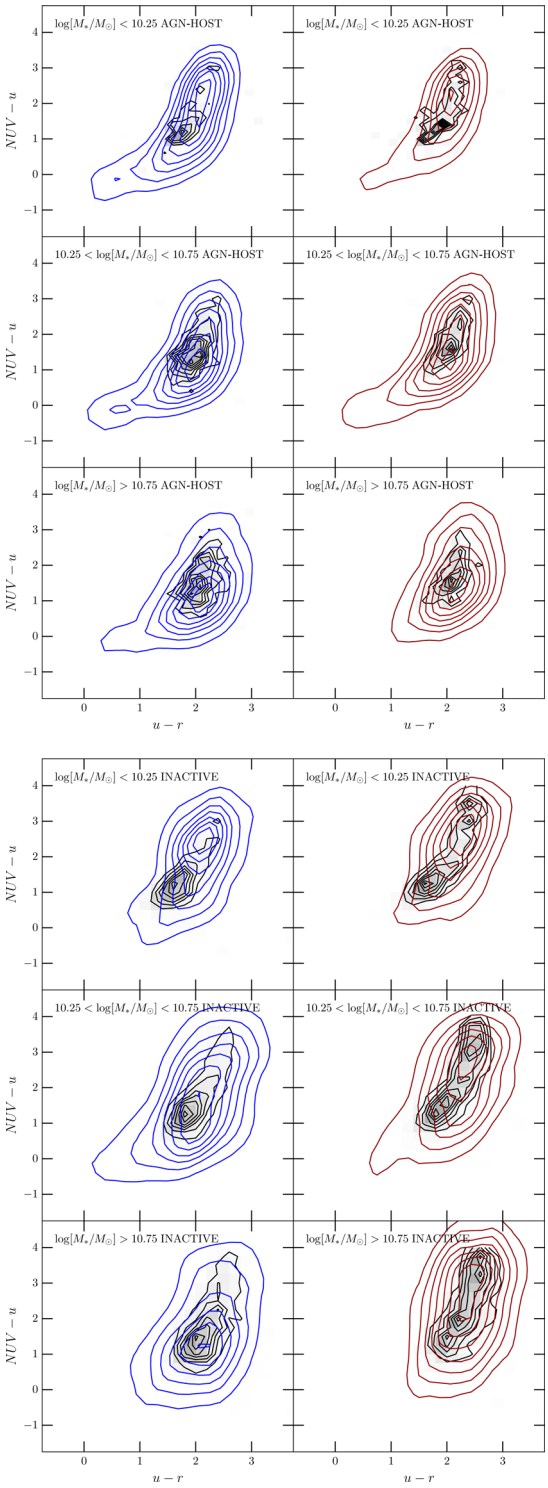

Figure C3. Optical-NUV colour–colour diagrams for the AGN-HOST (top) and INACTIVE (bottom) galaxies shown by the black contours, split into low-mass (top), medium-mass (middle) and high-mass (bottom) galaxies weighted by p_d (left) and p_s (right). Kernel smoothing has been applied to the overlaid replica data sets, which are created by sampling from the unweighted summed visualization distributions presented in Figs 4 and 5. Gaussian random noise is also added to the inferred colours, with a mean and standard deviation of the errors on the observed colours of the respective sample. Contours are shown for samples taken from the disc (blue) and smooth-weighted (red) summed visualization distributions.

This paper has been typeset from a TEX/LATEX file prepared by the author.